I. Rheology of Weakly Flocculated Suspensions of Rigid Particles

P. Snabre, P. Mills

I. Rheology of Weakly Flocculated Suspensions of Rigid Particles

P. Snabre ([1,*]) and P. Mills ([2])

([1]) Institut de Science et de génie des matériaux et procédés (**), B.P. 5, 66125 Font-Romeu, France
([2]) Université de Marne la Vallée (***), 2 rue du promontoire, 93166 Noisy le Grand, France

(Received 5 May 1995, revised 17 June 1996, accepted 11 September 1996)

PACS.47.50.+d – Non-Newtonian fluid
PACS.83.80.Lz – Biological materials: blood, collagen, wood, food, *etc.*
PACS.87.45.-k – Biomechanics, biorheology and biological fluid dynamics

Abstract. — A rheological law for hard spheres in purely hydrodynamic interaction is used to describe the steady state viscosity of weakly aggregated suspensions of rigid particles. The shear viscosity only involves the volume fraction and the maximum packing concentration of particles. Particle aggregation influences the parameters of the reference viscosity law. Within the framework of fractal aggregation, we introduce the volume fraction of aggregates and we derive the equilibrium mean radius of clusters from an effective medium approximation. The proposed rheological equation is close to the phenomenological Casson equation for soft clusters of fractal dimensionality $D = 2$. In a second part, we present rheo-optical experiments for studying the break-up of red cell aggregates in a shear flow and for determining the critical disaggregation shear stress of the flowing suspension mainly representative of the surface adhesive energy between particles. The proposed microrheological model well describes viscometric data in the low shear regime and allows information about the shear induced restructuration and the lifetime of clusters.

Résumé. — Nous utilisons une loi de viscosité pour des suspensions concentrées de sphères dures en interaction purement hydrodynamique pour décrire le comportement rhéologique des suspensions faiblement agrégées de particules rigides. La viscosité de cisaillement fait intervenir la fraction volumique et la concentration d'empilement des particules. La floculation des particules modifie les paramètres de la loi rhéologique. Dans le cadre de structures fractales, nous introduisons la fraction volumique effective des agrégats et nous déterminons la taille d'équilibre des amas à partir d'une hypothèse de milieu effectif. La loi de viscosité se rapproche de la loi phénoménologique de Casson pour des aggrégats mous de dimension fractale $D = 2$. Dans une seconde partie, nous présentons des expériences de réflectométrie sous cisaillement pour étudier la rupture des agrégats de globules rouges dans un écoulement et estimer la contrainte critique de désagrégation de la suspension représentative de l'énergie d'adhésion des particules. Le modèle rhéologique décrit les expériences de viscosimétrie à faible cisaillement et renseigne sur la restructuration des agrégats en écoulement et sur le temps de vie des amas réversibles.

(*) Author for correspondence (e-mail: snabre@imp-odeillo.fr)
(**) UPR 8521
(***) P.M.D. et URA 343 C.N.R.S.

1. Introduction

The prediction of suspension viscosity in concentrated systems is a long standing problem of important practical interest. Particulate suspensions and droplets dispersions such as paints, ink, food or biological systems show a variety of nonlinear rheological behavior in relation with the Brownian motion, the interparticle forces or the deformation of the particles in the flow. Repulsive interactions between particles may lead to quasi-crystal structures in concentrated systems while attractive forces induce the formation of clusters and continuous network above a gelation threshold. Non-Newtonian behavior of flocculated suspensions such as yield stress and shear thinning results from the rupture of the spanning network and finite clusters when increasing the shear stress [1]. Several authors have recently proposed microrheological models introducing the concept of fractal aggregation [2–8]. Mean field theories of aggregation and rupture of aggregates show a power law dependence of the viscosity on the shear rate. The rheological properties under steady-state conditions change until a dynamical equilibrium is established between the formation and break-up of aggregates. The deformation and orientation of elastic clusters and viscoelastic particles under flow may further account for the non-linear rheological properties of the suspension [9].

The first part of this work concerns the dynamical equilibrium and the steady-state shear-viscosity of an aggregated suspension of rigid particles assuming reversible floculation. The focus is on particles larger than one micron in diameter so that the hydrodynamic effects dominate over Brownian motion. Reynolds number for flow around immersed particles is further assumed small enough compared to unity for neglecting inertial effects relative to viscous forces.

Polymer bridging and phase separation induced by non-absorbing macromolecules usually produce reversible aggregates [6]. The structure of weakly flocculated suspensions is recovered rapidly after cessation of shear and repetitive experiments give reproducible data. However, bridging floculation in high molecular weight polymer solutions may produce irreversible clusters which structure is then determined by the rheological prehistory of the suspension [10]. Many numerical simulations and experiments suggest that aggregates behave as fractals on a scale larger than the primary particle size [11–13]. Taking into account the fractal properties of the clusters, we develop a model for cluster break-up during flow considering either rigid or soft reversible aggregates. We then deduce the equilibrium radius of interacting clusters from a mean field approximation assuming that the viscosity of the effective medium surrounding a cluster is the viscosity of the suspension. Using a viscosity law available for a suspension of randomly distributed hard spheres in purely hydrodynamic interactions, we finally introduce the effective volume fraction of aggregates and we derive an analytic dependence of the suspension viscosity on the shear rate. The proposed rheological equation only involves physical quantities in relation with the microscopic behavior of individual and interacting particles (the fractal dimension, the particle surface adhesive energy). The shear yield stress and the viscosity obtained from the model are then compared to rheological data obtained from the literature.

In this paper, we also present viscosity data for hardened red cell aggregates in a polymer solution (neutral dextran polymer). The break-up of red cell aggregates in Couette flow was further investigated by a laser light reflectometry technique. This rheo-optical method provides both a way for examining the effective medium approximation and estimating the critical disaggregation shear stress of the suspension. From the rheological equation and from estimates of the disaggregation shear stress, we can then describe the shear-thinning behavior of aggregated hardened red cells in the low shear regime.

In the last section, we further consider the shear-induced restructuration of aggregates and the finite lifetime of reversible clusters in relation with the rheological behavior of the suspension.

In a companion paper [61], we investigate the deformation and orientation of viscoelastic particles under shear flow in relation with the viscosity of the suspension and we finally propose a rheological equation for aggregates of deformable particles.

2. Viscosity of a Suspension of Unaggregated Hard Spheres

The viscosity of a suspension of monodispersed non-Brownian hard spheres in purely hydrodynamic interactions depends on the pair distribution function and may exhibit non-Newtonian behavior [15]. Neglecting normal stresses in a steady simple shear flow at low Reynolds number, the relationship between the viscous stress tensor and the rate of strain tensor involves a single viscosity coefficient:

$$\tau = \mu(\phi, \gamma)\gamma \tag{1}$$

where $\mu(\phi, \gamma)$ is the apparent shear viscosity of the suspension, ϕ the particle volume fraction and γ the apparent macroscopic shear rate. For dilute suspensions of hard spheres in a viscous fluid (viscosity μ_0), Batchelor and Green [15] extended the Einstein's formula [14] to second order in particle volume fraction:

$$\mu(\phi) = \mu_0 \left[1 + 2.5\phi + k\phi^2\right] \tag{2}$$

where the k coefficient depends on the flow field and the two-particle hydrodynamic interactions through the pair distribution function [15].

For concentrated systems of hard spheres in a viscous fluid, the basic problem for predicting the suspension viscosity is how to relate the microstructure configuration and the many-body hydrodynamic interactions. A mean field theory based on the estimation of the viscous dissipation in the fluid volume leads to an approximated expression of the relative shear viscosity [2,4,5]:

$$\mu_r\left(\phi, \phi_0^*\right) = \frac{\mu\left(\phi, \phi_0^*\right)}{\mu_0} = \frac{1-\phi}{\left(1-\phi/\phi_0^*\right)} \tag{3}$$

where ϕ_0^* is the critical volume fraction relative to the transition threshold between the fluid state and the solid state. For an isotropic pair distribution function in the low shear regime, the suspension displays a Newtonian behavior and the maximum packing volume fraction ϕ_0^* shows no dependence upon the shear rate. The apparent shear viscosity of the suspension then mainly depends on the maximum packing fraction. Shapiro and Probstein [16] indeed showed a correlation between the maximum random packing of the dry solid and the maximum packing fraction obtained from viscosity measurements for different bimodal size distributions.

As shown in Figure 1, equation (3) with the random isostatic packing fraction $\phi_i^* = 4/7$ for hard spheres well describes experimental data around the zero shear rate limit from Maron *et al.* [17], Krieger [18], De Kruiff *et al.* [19] and Gadala-Maria *et al.* [20].

However, a deviation occurs in the high concentration regime ($\phi > 0.5$, Fig. 1) which is likely associated with a change in the spatial distribution of particles and an increase in the maximum packing concentration. Computer simulations from Brady and Bossis [21] based on Stokesian dynamics indeed show the formation of transient shear-induced particle aggregates in concentrated systems of hard spheres. The volume fraction dependence of the shear viscosity yet displays no slope discontinuity since the life time of the finite transient structures remains short compared to the eddy diffusion time.

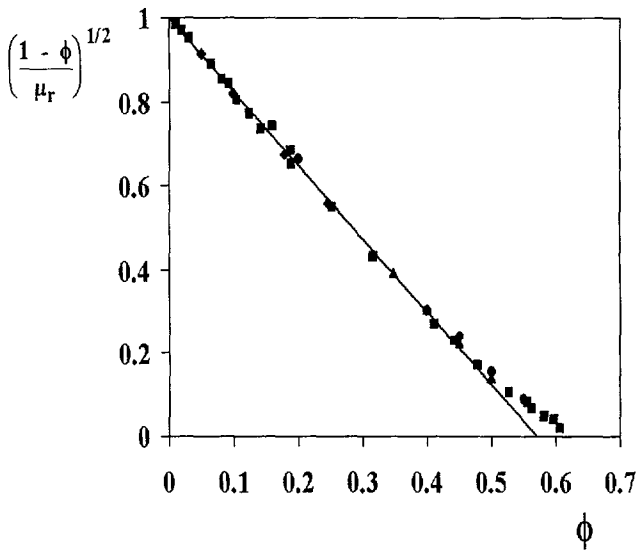

Fig. 1. — Experimentally observed values of $[(1-\phi)/\mu_r]^{1/2}$ around the zero shear rate limit for hard spheres in purely hydrodynamic interactions from Maron *et al.* (♦) [17], Krieger (△) [18], De Kruiff *et al.* (■) [19], Gadala-Maria *et al.* (●) [20]. Solid line is calculated from equation (3) with $\phi_0^* = 4/7$.

By considering the non-homogeneous and non-stationary features of viscous dissipation phenomena induced by the collisions of near-contact particles in the fluid phase and the emergence of lubrication forces in highly concentrated systems, a modified mean field theory then better describes the particle volume fraction dependence of the shear viscosity [22].

In the high shear rate regime, the shear forces between particles make the pair distribution function anisotropic along the main strain axes [23]. The flow-induced anisotropic microstructures (deformation and orientation of transient clusters in a shear flow) and the maximum packing fraction then closely depend on the interparticle potential and the flow type [24]. Therefore, no intrinsic expression for the shear viscosity can be established above a particle volume fraction of about 0.5 since both the shear rate and the rheological history of the suspension influence the spatial distribution of particles. At least, the viscosity of very concentrated suspensions in the vicinity of ϕ_0^* is certainly not relevant of mean field theories and perhaps would be better described with a central force percolation model. Up to now, this problem remains open.

In the case of a suspension of aggregated particles, the interparticle attractive forces between particles and/or clusters contribute to make the pair distribution isotropic and to inhibit the shear-induced clustering. Moreover, the polydispersity and the flexibility of irregularly shaped particles or clusters, as well as sedimentation effects are limiting factors for shear-induced ordering [25]. In the following and for volume fraction not too close to the maximum packing concentration ϕ_0^*, equation (3) is therefore assumed to be the reference rheological law for a random concentrated suspension of particles or permanent clusters, without dependence of the structure parameter ϕ_0^* upon the shear rate.

3. Structure of Cluster Suspensions in a Shear Flow

3.1. FRACTAL STRUCTURE OF AGGREGATES. — The first studies of aggregate formation date at least from the early work of Zsimondy (1901) on the floculation of gold colloids and from the classical theory of Von Smoluchowsky (1916) [60] on the kinetics of the irreversible cluster-cluster aggregation. In recent years there has been a strong resurgence of interest in this area with the work of Mandelbrot [26] about the fractal geometry and the experiments of Forest and Witten [27] showing that iron particle aggregates could be described as scale invariant objects called fractals. Several models of random cluster growth developed in the last decade and supported by numerical simulations lead to tenuous self-similar aggregates which radius of gyration $R_F(N)$ obeys the scaling relationship:

$$R_F(N) \approx aN^{1/D} \tag{4}$$

where N is the number of particles in the cluster, a the characteristic radius of elementary particles and D is called the fractal dimension or Hausdorf-Besicovitch dimension. A fractal dimension less than the Euclidean dimension d corresponds to open floc structures with porosity increasing with size. The Reaction Limited Aggregation model (RLA) by Kolb et Jullien [28] and Weitz and Huang [29] introduces a sticking probability when two clusters collide and covers reversible floculation. The RLA model produces self-similar clusters with a fractal dimension $D \approx 1.55$ for $d = 2$ and $D \approx 2$ for $d = 3$. For short range interactions, the lattice geometry and the dimensionality of aggregate trajectories (ballistic or random) hardly influence the long length scale structures in the cluster-cluster models [30,31]. On the other hand, selective break-up and regrowing of the aggregates in a flow may lead to structures of lesser porosity in later stages of cluster growth and produce denser flocs at high shear rates [13]. However, computer simulations introducing a restructuration process in RLA models such as random bond breaking or subcluster rotation only show a slight increase of the fractal dimensionality [32–34].

Finally, for reversible floculation in a shear flow, experimental and numerical investigations give a fractal dimensionality $2 < D < 2.3$ for three dimensional clusters [35,36] in rather good agreement with values from RLA models accounting for a restructuration process [34].

3.2. HYDRODYNAMIC RADIUS OF AGGREGATES. — The fluid draining of aggregates in a viscous flow is an important point in the rheology of a cluster suspension and determines the relation between the hydrodynamic radius and the gyration radius of tenuous structures [37]. Questions concerning the hydrodynamic interactions of a fractal aggregate may be answered in terms of the probability of intersection between two fractal clusters and a linear trajectory [26, 38]. The mean number of intersections between two clusters (mean gyration radius R) of fractal dimension D_1 and D_2 respectively (mean density ρ_1 and ρ_2) when they occupy the same region of space is roughly [26]:

$$M_{1,2} \approx \rho_1 \rho_2 R^d \approx R^{(D_1-d)} R^{(D_2-d)} R^d \approx R^{D_1+D_2-d} \tag{5}$$

Thus, in three dimension ($d = 3$), a linear trajectory of fractal dimensionality $\Delta = 1$ almost emerges from a large aggregate with fractal dimension $D < d - \Delta = 2$. In this case, the current line and the fractal cluster are mutually transparent and we may then consider a free draining approximation. On the other hand, a linear trajectory and a three dimensional cluster of fractal dimension $D > 2$ strongly interact. The interior fluid is trapped in the cluster and the exterior velocity profile is like the flow around a hard sphere with a radius R_F.

Typical reversible aggregates display a fractal dimension $D > 2$ and we may thus assume fractal clusters to behave hydrodynamically like compact spheres with an hydrodynamic radius

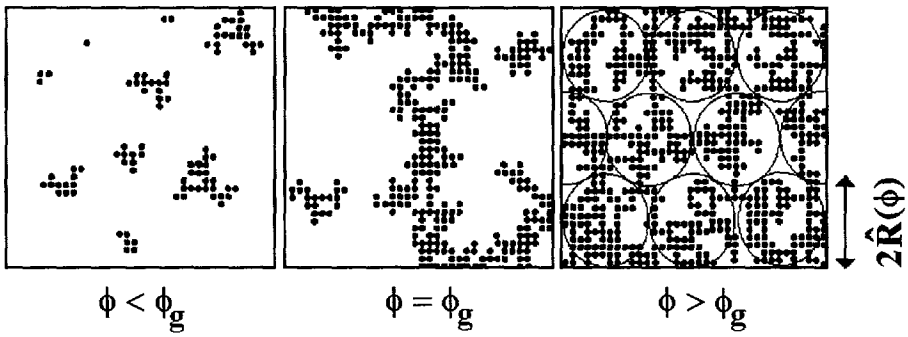

Fig. 2. — Structure of a floculated suspension at rest ($\phi < \phi_g$: finite sized clusters, $\phi = \phi_g$: an infinite spanning cluster and some isolated aggregates, $\phi > \phi_g$: packing of fractal "blobs" of dimension $\hat{R}_F(\phi)$).

equal to the radius of gyration [4,5]. This result is confirmed by recent calculations based on Stokesian dynamics of the drag coefficient for clusters with a fractal dimension $D \approx 2$ [39]. Branched neutral dextran polymers in a good solvent display a tenuous structure with a fractal dimension $D \approx 2.2$ and indeed present an hydrodynamic radius determined by gel permation chromatography very close to the gyration radius [40].

In fact, this result is only an approximation for large structures with extending loops since the penetration depth of fluid into such a tenuous object scales as the mean size of the heterogeneities near the outer surface. The assumption of unpermeable clusters is thus more realistic in concentrated suspensions since the aggregates strongly interpenetrate which reduces the effective mean radius of clusters.

3.3. Structure of Cluster Suspensions at Rest. — The mean particle volume fraction $\phi_F(N)$ in a fractal cluster decreases with the particle number belonging to the structure:

$$\phi_F(N) = \frac{Na^3}{R_F^3} \approx N^{\frac{D-3}{D}} \approx \left(\frac{R_F}{a}\right)^{D-3} \tag{6}$$

By increasing the concentration, the clusters cannot grow indefinitely without interpenetration. When the particle volume fraction is below the critical gelation concentration ϕ_g, the suspension only consists of isolated particles and finite sized clusters (Fig. 2).

Above the percolation concentration ϕ_g, cluster growth and overcrowding result in gelation and in the appearance of an infinite spanning structure. Fractal structures then fill space and reach a maximum mean radius $\hat{R}_F(\phi)$ at rest which decreases with particle volume fraction. Therefore, we may consider a concentrated suspension as a collection of fractal subclusters of mean density $\hat{\phi}_F$ and dimension $\hat{R}_F(\phi)$ packed with a volume fraction ϕ_0^* (Fig. 2). The filling space subclusters will be called "blobs" by analogy with the semi-dilute configuration of a polymer coil [41]. Neglecting the volume fraction of small aggregates located in between the blobs and considering equations (4) and (6), the maximum radius of fractal blobs at rest then obeys:

$$\phi = \hat{\phi}_F \phi_0^* \approx \frac{Na^3\phi_0^*}{\hat{R}_F(N)^3} \approx \phi_0^* \left(\frac{\hat{R}_F}{a}\right)^{D-3} \quad \text{for } \phi > \phi_g$$

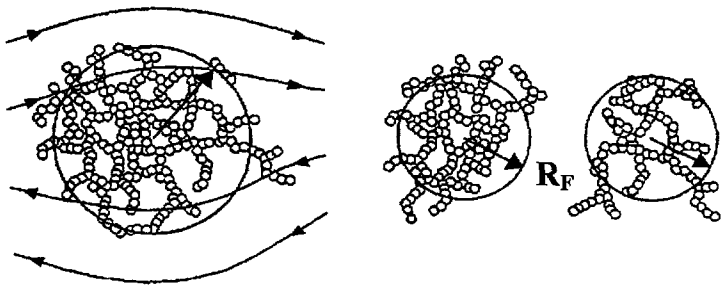

Fig. 3. — Shear break-up of a fractal cluster into approximately equal parts.

which finally gives:

$$\frac{\hat{R}_F}{a} = \left(\frac{\phi}{\phi_0^*}\right)^{-\frac{1}{3-D}} \tag{7}$$

For particle volume fraction close to the maximum packing fraction ϕ_0^*, the dimension of blobs tends toward the size of elementary particles and then a flowing floculated suspension behaves like an unaggregated system insofar as the lubrication forces dominate over the attractive forces for reversible aggregates.

3.4. Equilibrium Radius of Clusters in a Shear Flow. — Reversible clusters in a flowing suspension can grow until they reach a maximum stable size corresponding to a dynamical equilibrium between formation and break-up of the aggregates. An aggregate with radius above the maximum stable size is destroyed by shear stresses. An aggregate can break up into approximately equal parts (Fig. 3) or split off individual particles and small clusters one by one. The radius and shape of particles, the energy of links and both the type and strength of flow strongly influence cluster break-up [42, 43].

Experimental works [3, 12, 31] and computer simulations [34] suggest that the equilibrium radius $R_F(\tau)$ of an isolated fractal cluster decreases with increasing shear stress τ in form of a power law without dependence on the mean particle density in the aggregate:

$$\frac{R_F(\tau)}{a} \approx 1 + \left(\frac{\tau^*}{\tau}\right)^m \quad \text{with } 0.3 \leq m \leq 0.5 \tag{8}$$

where the characteristic shear stress τ^* for cluster break-up may be related to the surface adhesive energy Γ (adhesive energy per unit contact area):

$$\tau^* \approx \frac{\Gamma}{a} \tag{9}$$

Little is known about the exponent m which mainly depends on the reversibility of cluster deformation under the action of external stresses [34, 39]. Soft and rigid clusters represent extremes possible behavior of aggregates. A weak bonding energy (reversible floculation) gives rise to soft aggregates unable to transmit any elastic stresses then deforming irreversibly the internal structure. On the other hand, small elastic deformations preserves the structure of rigidly connected particles in relation with irreversible floculation.

In the general case, we may introduce a correlation length ξ under which the stress is transmitted and consider the cluster as a soft assembly of rigid subunits of radius ξ. In the

zero Reynolds number limit, an unpermeable aggregate of radius R_F experiences a viscous force:

$$F = \left| \int \overline{\overline{\tau}} \cdot \mathrm{d}s \right| \approx \tau R_F^2 \tag{10}$$

where $\overline{\overline{\tau}}$ is the viscous stress tensor and $|\mathrm{d}s|$ an outer surface element. This shear force exerts a bending moment $M \approx F\xi$ on the rigid branches of radius ξ located on the outer surface of the cluster. A bending moment $M^* \approx \tau^* a^3 \approx \Gamma a^2$ higher than the critical moment for breaking a cluster leads to the rupture of rigid subunits. The breaking criterion $F\xi \approx \Gamma a^2$ then gives the maximum stable radius $R_F(\tau)$ of unpermeable clusters in a shear flow:

$$\tau R_F^2 \xi \approx \Gamma a^2 \tag{11}$$

For soft clusters, the characteristic length ξ is of the same order as the particle radius a. Outer chains of mean radius $\xi \approx a$ are then stretched and broken one by one until the cluster reaches the maximum stable radius $R_F(\tau)$:

$$\frac{R_F(\tau)}{a} \approx 1 + \left(\frac{\tau^*}{\tau}\right)^{1/2} \quad \text{with } \tau^* \approx \frac{\Gamma}{a} \tag{12}$$

In the case of rigidly connected particles, the correlation length ξ is the whole radius of the aggregate ($\xi \approx R_F$) and then the structure is broken into approximately equal parts before reaching a stable size:

$$\frac{R_F(\tau)}{a} \approx 1 + \left(\frac{\tau^*}{\tau}\right)^{1/3} \quad \text{with } \tau^* \approx \frac{\Gamma}{a} \tag{13}$$

This result is consistent with the behavior of compact and rigid structures in a shear flow, where the average stress inside the aggregate scales as the cube of the linear dimension [39]. A value $m = 1/3$ is further in agreement with experimental data from Torres *et al.* [12] for rigid clusters. On the other hand, recent computer simulations of the break up of three dimensional soft aggregates gives $m = 1/2$ [34]. The previous considerations thus give a reasonable estimate of the exponent m varying from $m = 1/3$ for rigid clusters to $m = 1/2$ for soft aggregates. Of course, a mean field approximation is a crude estimate since the distribution of stress inside the aggregate certainly influences the condition for aggregate break up. However, computer simulations from Bossis *et al.* [39] based on Stokesian dynamics indicate that the stress distribution within a random cluster of fractal dimension $D \approx 2$ is rather flat which is coherent with the previous mean field approximation.

4. Shear Viscosity of Cluster Suspensions

4.1. Shear Yield Stress of an Aggregated Suspension. — Above the relation threshold ϕ_g, the rheological behavior of aggregated suspensions shows a yield stress under which the infinite spanning network no longer flows and displays solid-like viscoelasticity. For hydrodynamic conditions close to the shear yield stress τ_0, the maximum stable radius $R_F(\tau_0)$ of the aggregates equals the dimension $\hat{R}_F(\phi)$ of the filling space subclusters or "blobs". Relations (7) and (8) together with the condition $R_F(\tau_0) = \hat{R}_F(\phi)$ then gives an expression of the shear yield stress:

$$\tau_0 = \tau^* \left[\left(\frac{\phi}{\phi_0^*} \right)^{\frac{1}{D-3}} - 1 \right]^{-\frac{1}{m}} \quad \text{for } \phi > \phi_g \tag{14}$$

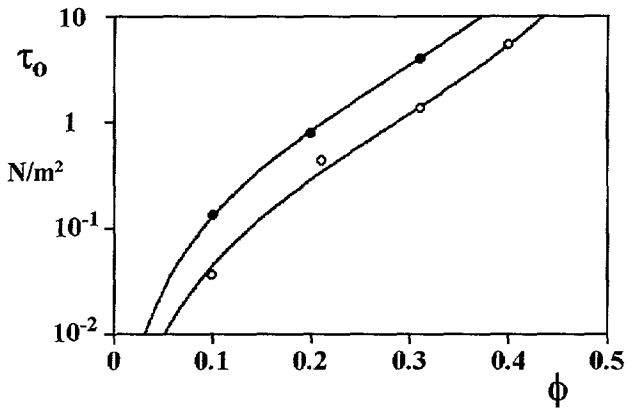

Fig. 4. — Particle volume fraction dependence of the shear yield stress τ_0. Experimental data from Choi and Krieger [44] for aggregated PMMA spheres in 50 cSt silicone fluid (●) or 200 cSt silicone fluid (○) (particle diameter 0.62 μm). Solid lines are obtained from equation (17) with $m = 1/2$, $D = 2$, $\phi_0^* = 4/7$ and $\tau^* = 1$ N m^{-2} or $\tau^* = 2.9$ N m^{-2}

In the semi-dilute regime $\phi_g < \phi \ll \phi_0^*$, the yield stress scales as:

$$\tau_0 \approx \frac{\Gamma}{a}\left(\frac{\phi}{\phi_0^*}\right)^{\frac{1}{m(3-D)}} \tag{15}$$

In the case of clusters of fractal dimension $D = 2$, the shear yield stress thus appears to scale like $\tau_0 \approx \Gamma\phi^\nu/a$ with $\nu = 3$ for rigid aggregates and $\nu = 2$ for soft structures. A limited number of data are available for the yield stress in shear flow and mainly concern colloidal particles. The experimental data from Buscall *et al.* [7] about the coagulation of polystyrene latex ($0.05 < \phi < 0.2$, particle diameter 0.49 μm) suggest a power law $\tau_0 \approx \tau^*\phi^3$ comparable to the scaling relation for rigid aggregates of fractal dimension $D = 2$. The experimental results from Choi and Krieger [44] for large clusters of PMMA spheres in silicone fluids are consistent with soft aggregates of fractal dimension $D = 2$. The depletion floculation of rigid particles in a weak minimum energy rather induces soft reversible clusters with a fractal dimension $D = 2$ (RLA model). As shown in Figure 4, relation (15) with $D = 2$ and $m = 1/2$ describes the volume fraction dependence of the yield stress for the depletion floculation of PMMA spheres in silicone fluids.

4.2. Shear Viscosity of Aggregated Suspensions. — For a fractal dimension $D > 2$, we may consider unpermeable fractal clusters with strong hydrodynamic screening inside the aggregate. Under steady state hydrodynamic conditions, we may further neglect the viscous dissipation in the interior fluid induced by the shear deformation of clusters. Above the yield stress, the clusters then behave like compact spheres of radius $R_F(\tau)$ and the viscous dissipation in the fluid between the aggregates determines the effective viscosity of the suspension. Therefore, we introduce the effective volume fraction ϕ_A of the aggregates and we use the reference law (3) for estimating the shear viscosity $\mu_A(\phi, \tau)$ of a cluster suspension:

$$\frac{\mu_A(\phi,\tau)}{\mu_0} = \frac{1-\phi_A}{\left(1-\phi_A/\phi_0^*\right)^2} \qquad \text{with} \qquad \phi_A = \phi\left[\frac{R_F(\tau)}{a}\right]^{3-D} \tag{16}$$

where ϕ_0^* is the maximum packing fraction of clusters.

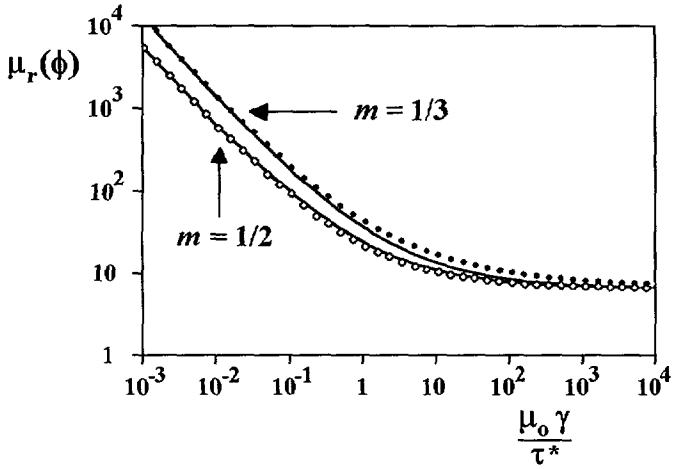

Fig. 5. — Theoretical relative shear viscosity $\mu_r = \mu_A/\mu_0$ of an aggregated suspension as a function of the dimensionless shear rate $\mu_0\gamma/\tau^*$ ($\phi = 0.4$ and $\phi_0^* = 4/7$). Casson law $\sqrt{\tau} = \sqrt{\tau_0} + \sqrt{\mu_D\gamma}$ (full lines) and equation (18) for either rigid clusters (●) or soft clusters (○) of fractal dimension $D = 2$. Equation (14) gives the shear yield stress $\tau_0(\tau^*, m)$.

The shear-thinning behavior of reversible floculated suspensions arises from the ability of clusters to screen the shear field and trap the interior fluid. In this sense, a collection of either compact clusters ($D = 3$) or free-draining aggregates of low fractal dimensionality behaves as an unaggregated suspension ($\phi_A = \phi$) and thus displays Newtonian properties.

Now, the problem is to estimate the cluster radius in a flowing suspension. For this purpose, we consider that interacting clusters behave like isolated aggregates in a fluid of viscosity equal to the shear viscosity of the suspension and thus experience an effective shear stress $\tau = \mu_A(\phi, \tau)\gamma$ [2–5]. Rheo-optical experiments presented in the following section confirm the effective medium approximation [43]. Equations (8) and (16) with the condition $\tau = \mu_A(\phi, \tau)\gamma$ then lead to a nonlinear expression of the effective viscosity:

$$\frac{\mu_A(\phi, \tau)}{\mu_0} = \frac{\tau}{\mu_0\gamma} = \frac{1 - \phi_A}{(1 - \phi_A/\phi_0^*)^2} \tag{17}$$

with $\phi_A \approx \phi\left[1 + \left(\frac{\tau^*}{\tau}\right)^m\right]^{3-D}$ For a fractal dimension $D = 2$, it follows from (14) and (17) that:

$$\sqrt{\tau}\left[1 - \left(\frac{\tau_0}{\tau}\right)^m\right] = \sqrt{\mu_D\gamma}\left[1 - \frac{\phi}{1-\phi}\left(\frac{\tau^*}{\tau}\right)^m\right]^{1/2} \tag{18}$$

where $\mu_D = \mu_0 \dfrac{1-\phi}{(1-\phi/\phi_0^*)^2}$ is the viscosity of the dispersed suspension in the high shear regime. The shear yield stress and thus the viscosity increase is higher for rigid structures than for soft aggregates (Fig. 5). The extreme case of soft clusters ($m = 1/2$) with a fractal dimensionality $D = 2$ leads to a Casson like behavior [1]:

$$\sqrt{\tau} = \sqrt{\tau_0} + \sqrt{\mu_D\gamma}\left[1 - \frac{\phi}{1-\phi}\left(\frac{\tau^*}{\tau}\right)^{1/2}\right]^{1/2} \tag{19}$$

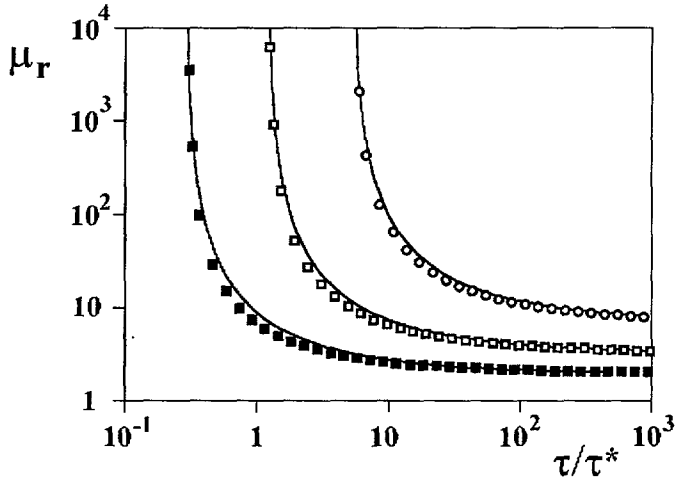

Fig. 6. — Theoretical relative shear viscosity $\mu_r = \mu_A/\mu_0$ of an aggregated suspension as a function of the dimensionless shear stress τ/τ^* for particle volume fraction $\phi = 0.2$ (■), $\phi = 0.3$ (□) and $\phi = 0.4$ (○) ($\phi_0^* = 4/7$). Casson law $\sqrt{\tau} = \sqrt{\tau_0} + \sqrt{\mu_D \gamma}$ (full lines) and equation (19) for soft clusters of fractal dimension $D = 2$. Equation (14) gives the shear yield stress $\tau_0(\tau^*, m)$.

with $\tau_0 = \tau^* \left(\frac{\phi_0^*}{\phi} - 1 \right)^{-2}$

As can be seen in Figures 5 and 6, a Casson law well approximates equation (19) since the last term approaches unity. The shear yield stress τ_0 to increases with the particle volume fraction and the asymptotic viscosity μ_D is reached above a critical shear stress $\tau_c \approx \alpha\tau^*$ representative of near complete disaggregation with $10^2 < \alpha < 10^3$ (Fig. 6).

A Casson equation also describes the rheological behavior of rigid clusters ($m = 1/3$) but underestimates the shear viscosity in the high shear regime (Fig. 5). Therefore, we may expect some information about the rigidity of particle clusters from the analysis of viscometric data under high shear rates $\gamma > \tau^*/\mu_0$. However, this approach based on fractal analysis ignores the particle shape details and becomes less predictive in the high shear regime where the disaggregation is almost complete.

Figure 7 shows the experimental data from Choi and Krieger [44] for aggregated suspensions of PMMA spheres (particle diameter 0.62 μm). The volume fraction dependence of the shear yield stress is coherent with soft clusters ($m = 1/2$) of fractal dimension $D = 2$ (Fig. 4). Equation (19) with $m = 1/2$ and $\tau^* = 1$ N m^{-2} describes the shear viscosity data over a large range of particle volume fraction (Fig. 7).

5. Viscosity of Aggregated Rigid Red Cells Suspensions

In this section, rheological experiments are reported for normal and hardened red cells in dextran saline solutions. After a recall of red cell properties and erythrocyte aggregation in dextran saline solution, we determine the fractal dimension of two-dimensional red cell aggregates and we investigate by a laser light reflectometric technique the effect of particle volume fraction and cell deformability on cluster break-up in shear flow. In the last section, we examine the viscometry data within the framework of the rheological model.

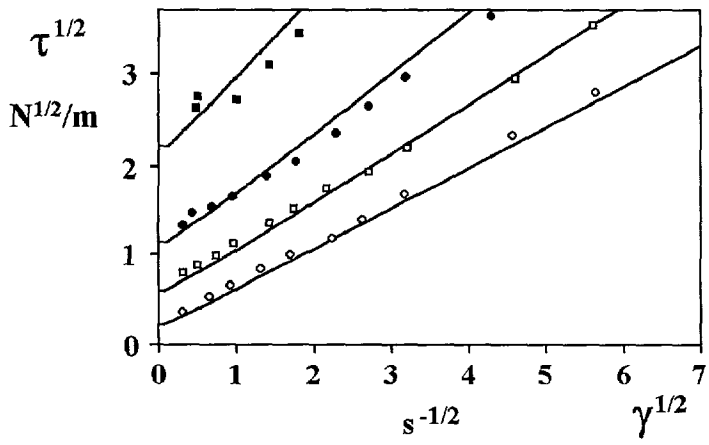

Fig. 7. — Rheological data from Choi and Krieger [44] for suspensions of aggregated PMMA spheres (particle diameter 0.62 μm) in 200 cSt silicone fluid ((○) $\phi = 0.1$, (□) $\phi = 0.21$, (●) $\phi = 0.31$, (■) $\phi = 0.4$). Solid curves are obtained from equation (19) with $m = 1/2$, $D = 2$, $\tau^* = 1$ N m^{-2}, $\mu_0 = 1.8$ Poise and $\phi_0^* = 4/7$.

5.1. Properties of Red Cell Aggregates. — Normal red cells or erythrocytes are biconcave disks of 8 μm in diameter and 2 μm thickness when in an isotonic phosphate buffered saline solution (osmolarity 300 mOsmol, ionic strength 150 mM and pH = 7.4) (Fig. 8a). The non-Newtonian behavior of blood arises from protein induced erythrocyte aggregation and cell deformability [45]. Red cells aggregate in the presence of macromolecules such as fibrinogen or high molecular weight dextrans [46]. Red cell elastic properties mainly arise from the underlying membrane structure or skeleton which consists of a continuous two dimensional ionic gel of spectrin-actin spanning the cytoplasmic surface of the membrane lipid bilayer [47]. Membrane glycoproteins and glycolipids further extend outside the cell forming an outer polymeric coat or glycocalyx (thickness 50 – 100 nm) carrying negative charges. Heat treatment of red cells induces irreversible alterations of the endoface membrane proteins and provides a way to alter membrane mechanical properties [48]. Crosslinking of the skeleton proteins in a glutaraldehyde solution produces hardened Red cells. The heating technique or the glutaraldehyde treatment have no significant influence on Red cell electrophoretic mobility and thus hardly alter the outer surface of the cell [48].

The whole blood of healthy donors is centrifuged three times (10 min at 3000 rpm) and then washed each time in PBS. The particle volume fraction is adjusted by microhematocrit technique. Heat treated Red cell were heated at constant temperatures (48.8 °C, 48.8 °C or 49.2 °C) for 2 min before rapid cooling to room temperature. Glutaraldehyde fixed red cells were prepared by suspending one volume of washed cells in 10 volumes of 2% glutaraldehyde saline solution for 60 min at room temperature. Hardened Red cells were then washed thrice in PBS. Finally, normal, heat treated or hardened cells are suspended in dextran saline solutions (ionic strength 150 mM).

Above a molecular weight of about 40 000, dextran polymer can induce red cell aggregation. The degree of cell aggregation then increases with molecular weight (Fig. 8). The onset of red cell aggregation occurs above a critical dextran concentration which is lower the higher the polymer molecular weight [5, 40, 49]. As dextran is added, the degree of cell aggregation increases and then decreases for polymer concentrations higher than 3–4 g%. The phenomenon

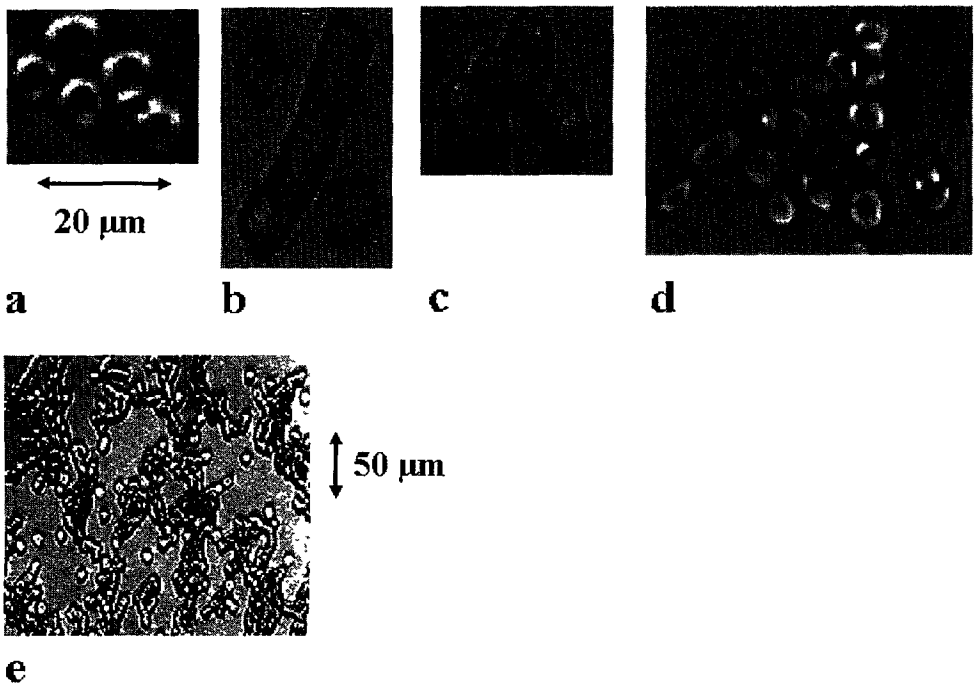

Fig. 8. — Pictures of normal red cells in phosphate buffered saline solution (a), 2 g% dextran 80-PBS (b,e) or 2 g% dextran 500-PBS (c) and hardened red cells in 2 g% dextran 80-PBS (d). Dextran 80 and 500 have molecular weight $M_w = 7.5 \times 10^4$ and $M_w = 5 \times 10^5$ [48].

of red cell aggregation is usually attributed to macromolecular bridging between cell surfaces [49]. However, the nature of red cell interaction in polymer solution remains controversial up to the present time. Indeed, there is good evidence that the disaggregation stage at high dextran concentrations arises from polymer depletion and penetration of dextran molecules within the cell surface coat [5].

During the aggregation process, deformable red cells maximize the contact area thus leading to roughly linear aggregates or rouleaux (Figs. 8b, c). Larger aggregates able to form a continuous network then consist of interconnected rouleaux (Fig. 8e). The equilibrium cell shape in the rouleaux results from the balance between the adhesive energy and the membrane strain energy. With increasing the surface adhesive energy, the curvature of the free surface of aggregated end cells then changes from concavity to convexity (Figs. 8b, c). On the other hand, hardened cells unable to deform only aggregate through contact points (Fig. 8d).

We have determined the fractal dimension of two-dimensional red cell aggregates. The method used is based on the imagery visualization of clusters between two glass plates after initial dispersion of the suspension. The cell number dependence of the cluster radius yields a fractal dimension $D = 1.59 \pm 0.03$ and $D = 1.56 \pm 0.04$ respectively for normal of hardened red cells in 3 g% dextran 80-PBS (Fig. 9). The nature of contact area between adjacent cells relevant to short range interactions and particle deformability only weakly influences the fractal dimensionality. However, deformable red cells show a large adhesive area and then give rise to somewhat denser clusters (Fig. 9). The fractal dimension $1.5 < D < 1.6$ of two dimensional red cell clusters is coherent with the predictions of the reaction limited aggregation model

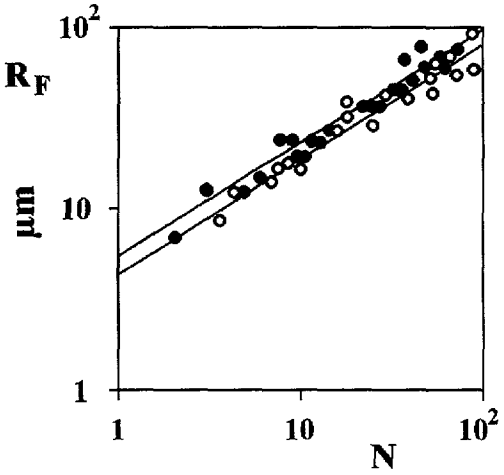

Fig. 9. — Log-log plot of the diameter of normal red cells (●) and hardened red cell aggregates (○) formed between two glass plates *versus* the number of constitutive cells. The straight lines are the best fit to the experimental data and lead to a fractal dimension $D = 1.59 \pm 0.03$ and $D = 1.56 \pm 0.04$ respectively for two dimensional normal and hardened red cell aggregates in 3 g% dextran 80-PBS. The average radius $R(N)$ of the red cell aggregates is determined by using the method from Allain and Jouhier [59].

($D \approx 1.55$ for $d = 2$) much more representative of reversible floculation. Therefore, we assume in the following a fractal dimension $D \approx 2$ for three dimensional red cell aggregates.

5.2. Packing Concentrations of Red Cells. — We have measured the shear viscosity of red cell suspensions at low shear rates in a Couette geometry with co-axial cylinders (Contraves LS30 low shear viscometer, controlled temperature 20 °C ± 0.2 °C). The calibration of the rheometer was performed with Newtonian silicone oils. The sample was stirred at a high shear rate before each measurement for avoiding sedimentation effects and the shear was further reduced to the value at which the measurement was performed. A new equilibrium was reached after some time and the viscosity was calculated from the steady-state torque readings. In repetitive experiments with a fresh sample, the procedure gives reproducible data with an error of about 4% for the relative shear viscosity.

At low shear stresses, suspensions of deformable or rigid red cells suspended in saline solution exhibit Newtonian behavior [45] since particles remain undeformed and present nearly random orientations in the shear field. However, the deformation-orientation of deformable cells at higher shear rates ($\gamma > 10$ s^{-1}) induces a shear-thinning rheological behavior [45]. On the other hand, the viscosity of hardened red cells in saline solution present no significant shear dependence at medium shear rates (0.01 s^{-1} $< \gamma <$ 130 s^{-1}, Figs. 14-16). We may thus consider a nearly random orientation distribution of unaggregated rigid cells in the flow without dependence upon shear rate.

The maximum packing concentration ϕ_0^* may be estimated from the viscosity data at low shear rates and the reference equation (3) for a suspension of unaggregated rigid particles. At low volume fraction, particles are randomly distributed and then the maximum packing fraction is close to the random isostatic packing $\phi_i^* \approx 4/7$ (Fig. 10). Above a critical volume fraction $\phi_c \approx \phi_i^* 3\ V/4\pi a^3 \approx 0.2$ ($V \approx 95\ \mu m^3$ is the red cell volume and $2a \approx 8\ \mu m$ the maximum

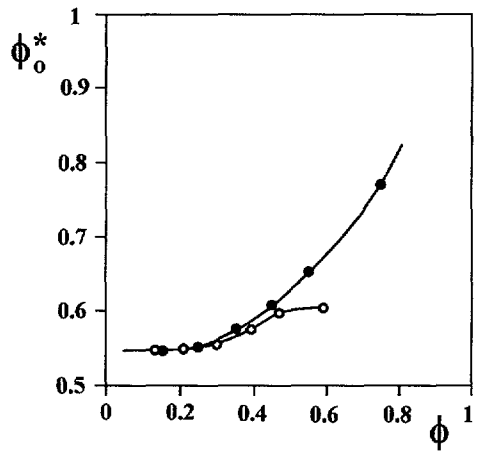

Fig. 10. — Maximum packing volume fraction ϕ_0^* of normal (●) and hardened red cells (○) derived from viscosity measurements at low shear rates as a function of particle volume fraction.

dimension of particles), the virtual spheres encircling the random collection of non spherical particles interpenetrate thus inducing a structuration of the suspension and an increase of the maximum packing fraction (Fig. 10).

For particle volume fraction above the random dense packing $\phi_d^* \approx 0.6$, hardened red cell suspensions no longer flow. On the other hand, suspensions of normal red cells remain fluid at high particle concentration since cell deformability allows membrane bending and motion of near contact particles. However, the flow induced deformation of cells in suspensions of closely packed particles then makes the viscosity at low shear rates and the maximum packing fraction strongly dependent upon the shear rate.

5.3. Shear Break-Up of Red Cell Aggregates. — In this part, we summarize results from a previous work [43] about the influence of particle volume fraction and membrane deformability on the shear break-up of red cell aggregates. We have investigated the shear dependence of both the apparent viscosity and the diffuse reflectivity of the flowing suspension. The special experimental set-up uses a rotational viscometer consisting of two coaxial cylinders (inner radius 10 mm and outer radius 11 mm), the larger of which is transparent and can rotate (Fig. 11). A Couette flow is established between the cylinders and the viscosity is calculated from the steady-state torque exerted on the inner cylinder. The suspension is probed by a He-Ne laser (wavelength $\Lambda = 6328$ Å and diameter 1 mm) that enters perpendicularly to the flow direction. The light flux $I(\theta)$ backscattered by the flowing suspension is detected at small angles ($10° < \theta < 20°$) by a photometric device (Fig. 11).

Ignoring polarization, inelastic scattering and fluorescence, radiative transfer phenomena can be described by a limited number of parameters: the mean free path λ (the mean distance between scattering events), the probability K of photon absorption between successive scatterings and the anisotropy coefficient g (average cosine of the single particle scattering angle) [50,51]. For large particles such as red cells with a size parameter $\pi d/\Lambda > 10$, the scattered energy per unit volume (efficiency factor) is $Q_d \approx 2$ and the mean free path scales as the inverse of the scattering area per unit volume [52]:

$$\lambda = \frac{2}{\sigma} \tag{20}$$

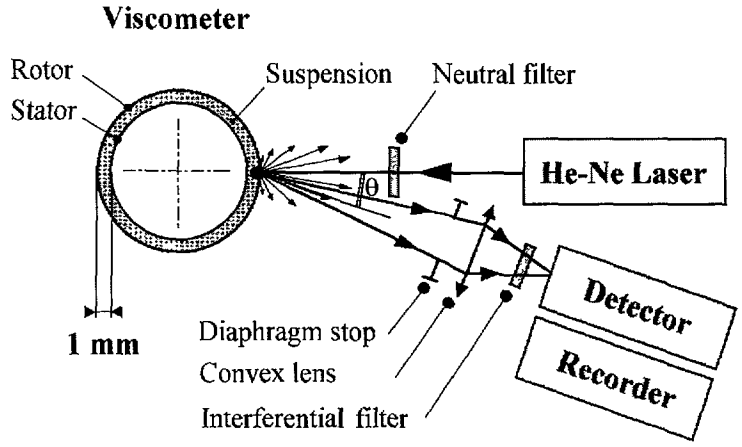

Fig. 11. — Schematic illustration of the rheo-optical technique for measuring the diffuse reflectivity of a suspension in a Couette flow.

The classical relation from Kubelka and Munk [53, 54] gives a scaling law for the diffuse reflectivity $r(K, g)$ of an optically thick medium consisting of weakly absorbing and randomly distributed scatterers [5, 50]:

$$\frac{(1-r)^2}{r} \approx \frac{2\beta}{f} \approx \frac{K}{\varphi(g)} \qquad \text{for} \qquad K \ll 1 \tag{21}$$

where $\beta \approx K/\lambda$ and $f \approx \sigma\varphi(g) \approx \varphi(g)/\lambda$ are the absorption and scattering coefficients per unit length. For red cell suspensions probed by a He-Ne laser, backscattering experiments lead to $K \approx 3 \times 10^{-3}$ and $g \approx 0.9927$ [50]. Thus, we may use the relation (21) because of the weak absorption of light by red cells ($K \ll 1$).

Electron microscopic pictures of red cell aggregates in dextran saline solutions show a relatively uniform gap between adjacent cell surfaces [49] accross which the light is not scattered since the intercellular distance of about 200 Å is much lower than the wavelength of the incident radiations. Red cell aggregation thus lowers the scattering area per unit volume and causes a decrease in the isotropic backscattered flux. The absorption parameter K_A for an aggregated red cell suspension scales as the scattering mean free path λ_A and then obeys the relation:

$$\frac{K_A}{K} = \frac{\lambda_A}{\lambda} = \frac{\sigma}{\sigma - \sigma_A} \qquad \text{with} \qquad \lambda_A = \frac{2}{\sigma - \sigma_A} \tag{22}$$

where σ_A is the total cell area participating in intercellular adhesion per unit volume of the suspension. Assuming the asymmetry factor g_A of red cell aggregates very close from that of randomly distributed particles ($g_A = g$), we may estimate the diffuse reflectivity r_A of an optically thick aggregated red cell suspension from the relations (21) and (22):

$$\frac{(1-r_A)^2}{(1-r)^2}\frac{r}{r_A} \approx \frac{K_A}{K} \approx \frac{\sigma}{\sigma - \sigma_A} \tag{23}$$

where r and σ are the diffuse reflectivity and the scattering area per unit volume of an optically thick suspension of randomly distributed and unaggregated red cells. Since $r_A < r \approx 0.15$ for

oxygenated red cells [50], we can then approximate to good accuracy the relative reflectivity r_A/r in (25) by $(\sigma - \sigma_A)/\sigma$ and define the reflectometric index G:

$$G = 1 - \frac{r_A}{r} \approx \frac{\sigma_A}{\sigma} \tag{24}$$

The relative scattered intensity r_A/r shows no dependence on the scattering angle since the great number of scattering events randomizes the backscattered flux [5, 50]. Considering the relative diffuse reflectivity r_A/r further reduces the influence of both cell oxygenation and internal reflections on the intensity of the backscattered flux. The reflectometric index G thus provides a measure of the red cell aggregation degree and is suitable for interpreting the reflectivity measurements in a simple shear flow since the scattering area is nearly uniform accross the gap.

We have measured the diffuse reflectivity of normal and heat treated red cells suspended in dextran saline solutions. The reflectometric index G decreases when the shear rate is raised above 1 s^{-1}, indicating a progressive shear-induced dispersion of red cell clusters into smaller ones (Figs. 12). Under defined shear rate conditions, particle crowding and cell rigidity increases the viscosity of the suspension and improves the dissociation efficiency of the flow, resulting in a lower reflectometric index [43]. When plotting the reflectometric data *versus* the shear stress $\tau = \mu_A(\gamma)\gamma$, we obtain a single curve without significant dependence upon particle volume fraction (Fig. 12a) or cell deformability (Fig. 12b). Deformable and nearly-rigid red cell aggregates thus obey the same breaking-up behavior in a simple shear flow and may be considered as soft clusters. Under the action of external stresses, rigid red cell clusters indeed undergo irreversible deformation since the rigid biconcave particles can roll at their contact point.

The effective shear stress τ and the surface adhesive energy Γ determine the aggregation degree $\sigma_A(\tau)/\sigma$ of the suspension and the mean radius $R(\tau, \tau^*)$ of flowing clusters in agreement with relations (8) and (9). The critical disaggregation shear stress τ_c defined in terms of extrapolated intercept (Figs. 12) is representative of near complete cell dispersion and directly reflects the mechanical force required to break the adhesive bonds between two particles.

According to the Derjaguin theory, the critical force $F_c \approx \tau_c a^2$ required to break a doublet scales as Γa [55] and the critical shear stress τ_c for nearly complete particle disaggregation in a shear flow then takes the form:

$$\tau_c \approx \frac{\Gamma}{a} \tag{25}$$

For cells in 2 g% dextran 80-PBS ($\tau_c \approx 0.55$ N m^{-2}, Fig. 12b), we calculate from equation (25) a surface adhesive energy $\Gamma \approx 2 \times 10^{-6}$ N m^{-1} taking $a \approx 4$ μm for the characteristic radius of red cells. This value agrees fairly well with earlier estimations of the surface adhesive energy based on equilibrium doublet shape and membrane properties [56]. It is interesting to note that the mean critical disaggregation shear stress of red cells in human plasma is about $\tau_c \approx 0.45$ N m^{-2} [43] indicating that human blood displays an aggregation behavior very similar to red cells in 2 g% dextran 80-PBS.

The characteristic shear stress $\tau^* \approx \Gamma/a$ for cluster break-up involved in the rheological model (8-9) scales as the critical shear stress τ_c ($\tau^* = \alpha\tau_c$). Reflectometric experiments thus provide a way for estimating the surface adhesive energy Γ and for determining the critical disaggregation shear stresses $\tau_c(\Gamma)$ and $\tau^*(\Gamma)$ representative of the physicochemical interactions between particles. The critical disaggregation shear stress increases with dextran molecular weight (Fig. 13) indicating a higher adhesive surface energy.

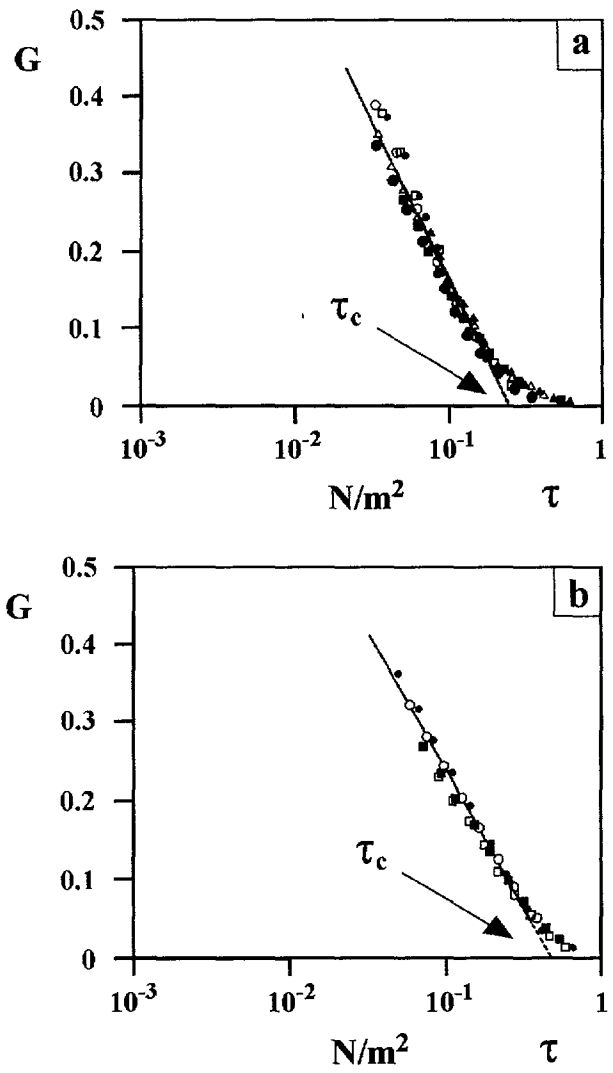

Fig. 12. — Reflectometric index G against the shear stress in a Couette flow for normal red cells in 1.2 g% dextran 80-PBS ((○) $\phi = 0.15$, (•) $\phi = 0.25$, (□) $\phi = 0.35$, (●) $\phi = 0.45$, (△) $\phi = 0.55$, (■) $\phi = 0.65$, (△) $\phi = 0.75$) or heat-treated red cells in 2 g% dextran 80-PBS ((•) normal cells, (○) $T = 48.4$ °C, (■) $T = 48.8$ °C, (□) $T = 49.2$ °C).

5.4. Viscosity of Hardened Red Cell Suspensions. — In this section, we present viscometric data for rigid red cells in dextran saline solutions. The hardened red cell suspensions were previously dispersed by shearing at 130 s^{-1} and then allowed to relax for 5 minutes. Steady shear experiments were performed by increasing the shear rate step by step and waiting for steady state before the measurement. Figures 14-16 show the experimental data when varying the particle volume fraction, the dextran molecular weight and the polymer concentration in the suspending fluid.

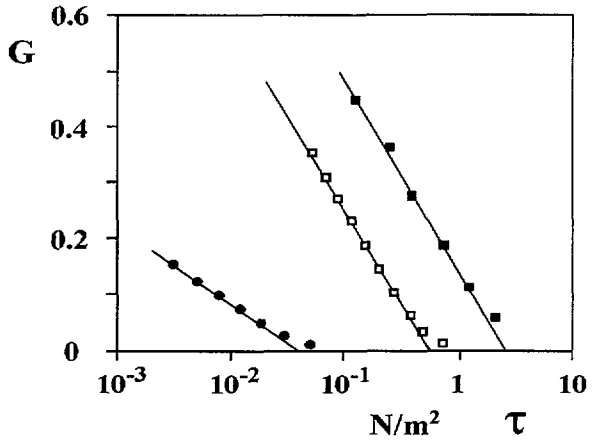

Fig. 13. — Reflectometric index G against the shear stress in a Couette flow for normal red cells in 2 g% dextran 40-PBS (●), 2 g% dextran 80-PBS (□) and 2 g%dextran 150-PBS (■). The particle volume fraction is $\phi = 0.45$ and the critical disaggregation shear stress τ_c is derived from extrapolated intercept.

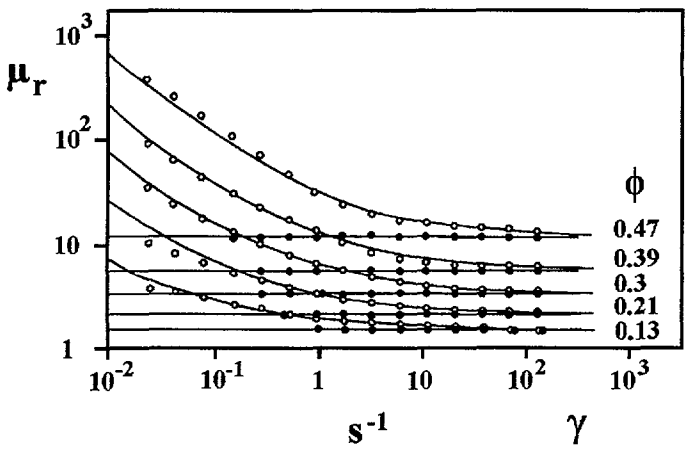

Fig. 14. — Relative shear viscosity $\mu_r(\phi) = \mu_A(\phi)/\mu_0$ of hardened red cells suspended in saline solution (●) or in 2 g% dextran 80-PBS (○). The solid curves are calculated from the relation (19) with $D = 2$, $m = 1/2$ and $\tau^* = \tau_c/600$. The critical disaggregation shear stress $\tau_c = 0.55$ N m^{-2} is determined from the reflectometric curves $G(\tau)$ and the maximum packing fraction $\phi_0^*(\phi)$ is derived from the shear viscosity of unaggregated particles.

The maximum packing fraction ϕ_0^* was derived from the reference law (3) and the shear viscosity measurements of rigid red cells suspended in saline solution (Fig. 10). The critical disaggregation shear stress τ_c was further determined in terms of extrapolated intercept by plotting the shear stress dependence of the reflectometric index $G(\tau)$ (Figs. 12-13).

Assuming soft clusters ($m = 1/2$) of fractal dimension $D = 2$ and taking a characteristic shear stress $\tau^* = \tau_c/600$, the rheological law (19) for a concentrated suspension of reversible clusters well describes the viscometric experiments in the low shear regime (Figs. 14-16).

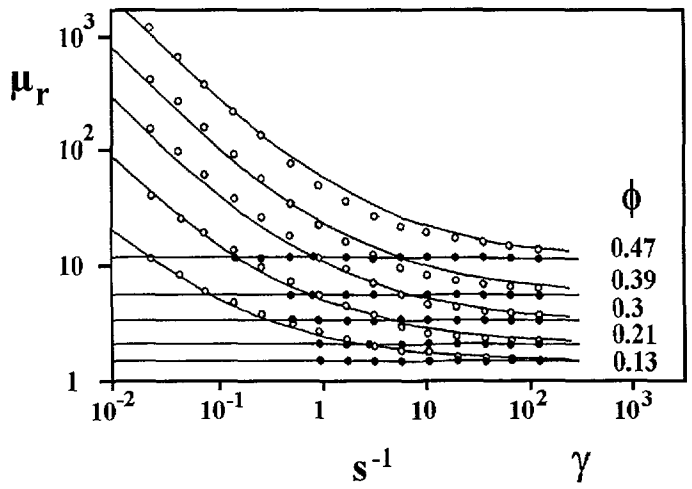

Fig. 15. — Relative shear viscosity $\mu_r(\phi) = \mu_A(\phi)/\mu_0$ of hardened red cells suspended in a saline solution (●) or in 2 g% dextran 150-PBS (○). The solid curves are calculated from the relation (19) with $D = 2$, $m = 1/2$ and $\tau^* = \tau_c/600$. The critical disaggregation shear stress $\tau_c = 2.5$ N m^{-2} is determined from the reflectometric curves $G(\tau)$ and the maximum packing fraction $\phi_0^*(\phi)$ is derived from the shear viscosity of unaggregated particles.

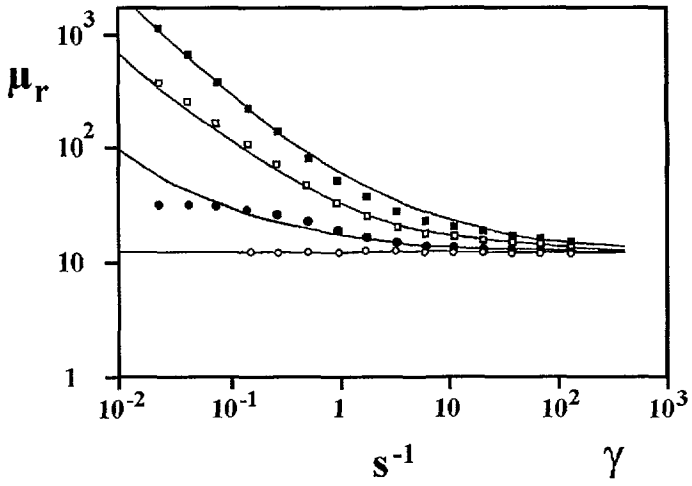

Fig. 16. — Relative shear viscosity of $\mu_r(\phi) = \mu_A(\phi)/\mu_0$ hardened red cells suspended in saline solution (○), 2 g% dextran 40-PBS (●), 2 g% dextran 80-PBS (□) and 2 g% dextran 150-PBS (■) with a particle volume fraction $\phi = 0.47$. The solid curves are calculated from the relation (19) with $D = 2$, $m = 1/2$, $\phi_0^* = 0.595$ and $\tau^* = \tau_c/600$. The critical disaggregation shear stress is determined from the reflectometric curves $G(\tau)$ ($\tau_c = 0.04$ N m^{-2} for 2 g% dextran 40, $\tau_c = 0.55$ N m^{-2} for 2 g% dextran 80 and $\tau_c = 2.5$ N m^{-2} for 2 g% dextran 150).

However, the model weakly overestimates the shear viscosity in the medium shear regime ($1\ s^{-1} < \gamma < 10\ s^{-1}$) for high particle volume fractions and strong adhesive energies (Figs. 15-16). This deviation may arise from a multilevel floc structure with small clusters of lesser porosity.

The shear induced formation of compact aggregates also may explain the observed reduced viscosity in the intermediate shear regime for strongly aggregated rigid particles [57]. The preferential breakage of weak parts of the clusters and the increase of contact points between particles may lead to the formation of lesser porosity aggregates [13,58].

A restructuration process requires a significant increase of the internal energy $E \approx Nze$ of the aggregate (z is the mean coordination number or the mean number of contacts around every particle, $e \approx \Gamma s$ the bond adhesive energy and s the contact area between aggregated particles). Particle crowding and cell adhesiveness thus promote a shear compaction of the aggregates in a flow. However, contact points between aggregated rigid particles ($s \to 0$) result in a weak bond energy e and small variations of the internal energy $E(N, e)$ of the aggregates thus limiting the extent of the shear induced restructuration phenomena. For aggregated rigid red cells, viscosity experiments indeed show no significant hysteresis or memory effects when increasing or decreasing the flow step by step in the low shear regime.

On the other hand, the aggregation of deformable cells leads to a large adhesive area between adjacent membranes and a higher bond energy. The cell deformability and the significant variation in the internal energy of the aggregates then allows a shear restructuration of the suspension giving rise to noticeable hysteresis and memory effects [5,61].

In contrast with the predictions of the model, the shear viscosity further keeps a nearly constant value in the low shear regime for weakly aggregated rigid red cells in 2 g% dextran 40-PBS (Fig. 16). The stresses associated to Brownian motion and particle sedimentation may limit the lifetime of reversible clusters and then the suspension consists of isolated finite sized clusters unable to reach the maximum radius $\hat{R}_F(\phi)$ and to form an infinite spanning structure above the percolation concentration. The mean lifetime of a cluster scaling as t_0/N (t_0 is the mean lifetime of a bond and N the particle number), we may define a Deborah number $\gamma t_0/N$ with respect to the characteristic time $1/\gamma$ of the flow. At high shear rates, the mean size of clusters is controlled by shear forces when the time scale $1/\gamma$ is larger than the finite lifetime t_0/N of the aggregates. On the other hand, the mean lifetime t_0 of adhesive bonds determines the cluster radius $R(t_0)$ and the viscosity of the suspension in the low shear regime (low values of the Deborah number). Such a situation arises for a weak aggregation of particles in the diluted regime (associated with high values of the maximum radius $\hat{R}_F(\phi)$) and explains the disappearance of the yield stress rheological behavior.

6. Conclusion

We have proposed a microrheological model for weakly aggregated suspensions using the concept of fractal clusters. The mean size of reversible fractal aggregates in a shear flow is derived from a mean field approximation assuming that the viscosity of the effective medium surrounding a cluster is the viscosity of the suspension. The flow dependent changes of the diffuse reflectivity of red cell suspensions are shown to be coherent with the effective medium approximation. Rheo-optical experiments further provide a powerfull means for determining the critical disaggregation shear stress mainly representative of the surface adhesive energy, independently of particle volume fraction and cell deformability. From the estimate of the critical disaggregation shear stress, the proposed theory well describes the viscosity data in the low shear regime for hardened red cells in dextran polymer solutions and allows information about the rigidity and the fractal dimensionality of clusters. In the high shear regime, the maximum

packing fraction describes particle shape effects and determines the shear viscosity of the suspension. The restructuration of clusters in shear flow and the finite lifetime of adhesive bonds however may influence the rheological behavior of weakly aggregated suspensions.

References

[1] Casson N., A flow equation for pigment-oil suspensions of printing ink type. In Rheology of disperse systems, C.C.Mills, Ed. (Pergamon, 1959) pp. 84-102.

[2] Mills P., Non-Newtonian behavior of flocculated suspensions, *J. Phys. Lett. France* **46** (1985) L301-309.

[3] Sonntag R.C. and Russel W.B., Structure and breakup of flocs subjected to fluid stresses, *J. Colloid Interface Sci.* **115** (1987) 378-389.

[4] Mills P. and Snabre P., The fractal concept in the rheology of concentrated suspensions, *Rheol. Acta* **26** (1988) 105-108.

[5] Snabre P., Rhéologie des suspensions concentrées et agrégées de particules déformables. Application à la suspension sanguine. Thèse d'état (Université Paris VII, 1988).

[6] Patel P.D. and Russel W.B., The rheology of polystyrene latices phase separated by dextran, *Colloids and surfaces* **31** (1988) 355-383.

[7] Buscall R., Mills P.D.A., Goodwin J.W. and Lawson D.W., Scaling behaviour of the rheology of aggregate networks formed from colloidal particles, *J. Chem. Soc. Faraday Trans.* **84** (1988) 4249-4260.

[8] Wessel R. and Ball R.C., Fractal aggregates and gels in shear flow, *Phys. Rev. A* **46** (1992) R3008-3011.

[9] Barthes-Biesel D. and Chim V., Constitutive equation of a dilute suspension of spherical microcapsules, *Int. J. Multiphase Flow* **7** (1981) 473-493.

[10] Firth B.A. and Hunter R.J., Flow properties of coagulated colloidal suspensions, *J. Colloid Interface Sci.* **57** (1976) 266-275.

[11] Schaefer D.W., Martin J.E., Wiltzius P. and Cannell D.S., Fractal geometry of colloidal aggregates, *Phys. Rev. Lett. France* **52** (1984) 2371-2374.

[12] Torres F.R., Russel W.B. and Schowalter W.R., Simulations of coagulation in viscous flows, *J. Colloid Interface Sci.* **145** (1991) 51-73.

[13] Oles V., Shear-induced aggregation and breakup of polystyrene latex spheres, *J. Colloid Interface Sci.* **154** (1992) 351-358.

[14] Einstein A., *Ann. Phys.* **19** (1906) 1989 and *ibid* **34** (1911) 591.

[15] Batchelor G.K. and Green J.T., The determination of the bulk stress in a suspension of spherical particles to order c^2, *J. Fluid Mech.* **56** (1972) 401-427.

[16] Shapiro A.P. and Probstein R.F., Random packing of spheres and fluidity of monodisperse and bidisperse suspensions, *Phys Rev. Lett. France* **68** (1992) 1422-1425.

[17] Maron S.H. and Levy-Pascal A., Rheology of synthetic latex, *J. Colloid Sci.* **10** (1955) 494-503.

[18] Krieger I.M., Rheology of monodisperse lattices, *Advan. Colloid Interface Sci.* **3** (1972) 111-136.

[19] De Kruiff C.G., Van Iersel E.M.F. and Vrij A., Hard sphere colloidal dispersions: Viscosity as a function of shear rate and volume fraction, *J. Chem. Phys.* **83** (1985) 4717-4725.

[20] Gadala-Maria and Acrivos A., Shear-induced structure in a concentrated suspension of spheres, *J. Rheol.* **24** (1980) 799-814.

[21] Brady J.F. and Bossis G., Stokesian dynamics, *Ann. Rev. Fluid Mech.* **20** (1988) 111-157.
[22] Mills P. and Snabre P., Rheology and structure of concentrated suspensions of hard spheres. Shear induced particle migration, *J. Phys. II France* **5** (1995) 1997-1608.
[23] Parsi F. and Gadala-Maria F., Fore-and-aft asymmetry in a concentrated suspension of spheres, *J. Rheol.* **31** (1987) 725-732.
[24] Petit L., Ecoulement et mise en structure de suspensions macroscopiques, *Ann. Phys. Fr.* **16** (1991) 155-191.
[25] Wagner N.J. and Russel W.B., Light scattering measurements of a hard sphere suspension under shear, *Phys. Fluids A* **2** (1990) 491-502.
[26] Mandelbrot B.B., The fractal geometry of nature (Freeman, NY, 1982).
[27] Forrest S.R. and Witten T.A., Long-range correlations in smoke-particle aggregates, *J. Phys. A* **12** (1979) L109-117.
[28] Kolb M. and Jullien R., Chemically limited versus diffusion limited aggregation, *J. Phys. Lett. France* **45** (1984) L977-981.
[29] Weitz D.A. and Huang J.S., in Aggregation Gelation, F. Family and D.P. Landau, Eds., vol. 19 (North Holland, Amsterdam, 1984).
[30] Meakin P., Computer simulation of cluster-cluster aggregation using linear trajectories, *J. Colloid Interface Sci.* **102** (1984) 505-512.
[31] Torres F.R., Russel W.B. and Schowalter W.R., Simulations of coagulation in viscous flows, *J. Colloid Interface Sci.* **145** (1991) 73-85.
[32] Meakin P. and Jullien R., Structural readjustment effects in cluster-cluster aggregation, *J. Phys. France* **46** (1985) 1543-1552.
[33] Meakin P. and Jullien R., The effects of restructuring on the geometry of clusters formed by diffusion-limited, ballistic, and reaction-limited cluster-cluster aggregation, *J. Chem. Phys.* **89** (1988) 246-250.
[34] Potanin A.A., On the computer simulation of the deformation and breakup of colloidal aggregates in shear flow, *J. Colloid Interface Sci.* **157** (1993) 399-410.
[35] Schaeffer D.W. and Keefer K.D., Fractal geometry of silica condensation polymers, *Phys. Rev. Lett.* **53** (1984) 1383-1386.
[36] Stoll S., Elaissari A. and Pefferkorn E., Fractal dimensions of latex aggregates: correlation between hydrodynamic radius and cluster size, *J. Colloid Interface Sci.* **140** (1990) 98-104.
[37] Adler P.M. and Mills P., Motion and rupture of a porous sphere in a linear flow field, *J. Rheol.* **23** (1979) 25-37.
[38] Witten T.A. and Cates M.E., Tenuous structure from disorderly growth processes, *Science* **282** (1986) 1607-1612.
[39] Bossis G., Meunier A. and Brady J.F., Hydrodynamic stress on fractal aggregates of spheres, *J. Chem. Phys.* **94** (1991) 5064-5070.
[40] Snabre P., Grossman G. and Mills P., Effects of dextran polydispersity on red blood cell aggregation, *Colloid Polym. Sci.* **263** (1985) 478-483.
[41] De Gennes P.G., Scaling concepts for polymer physics (Cornell Univ. Press, NY, 1979).
[42] Van De Ven T.G.M., Colloidal Hydrodynamics (Academic Press Inc., 1989).
[43] Snabre P., Bitbol M. and Mills P., Cell disaggregation behavior in shear flow, *Biophys. J.* **51** (1987) 795-807.
[44] Choi G.N. and Krieger I.M., Rheological studies on sterically stabilized dispersions of uniform colloidal spheres. II Steady shear viscosity, *J. Colloid Interface Sci.* **113** (1986) 101-113.
[45] Goldsmith H.L. and Mason S.G., The microrheology of dispersions. Eirich F.R., Ed. (N.Y. Academic, 1982) pp. 86-250.

[46] Jan K.M., Red cell interactions in macromolecular suspension, *Biorheology* **16** (1979) 137-148.
[47] Evans E.A. and Skalak R., Merchanics and thermodynamics of biomembranes (C.R.C. Press, Inc, Boca Raton, 1980).
[48] Snabre P., Baumler H. and Mills P., Aggregation of human R.B.C. after heat treatment. *Biorheology* **22** (1985) 185-195.
[49] Chien S. and Jan K.M., Red cell aggregation by macromolecules. Roles of surface adsorption and electrostatic repulsion, *J. Sup. Structure* **1** (1975) 385-409.
[50] Gandjbackche A.H., Mills P. and Snabre P., Laser light technique for the study of orientation and deformation of viscoelastic particles in a Couette flow, *App. Opt.* **33** (1994) 1070-1079.
[51] Pine D.J., Weitz D.A., Maret G., Wolf P.E., Herbolzheimer E. and Chaikin P.M., In Scattering and localization of classical waves in random media, Ping Sheng, Ed., (World Scientific, 1990).
[52] Borhen C. and Huffman D.R., Absorption and scattering of light by small particles (J. Wiley & Sons, Ed., 1983).
[53] Kubelka P. and Munk F., Isotropic multiple light scattering in a suspension, *J. Opt. Soc. Am.* **38** (1948) 448.
[54] Van De Hulst H.C., Multiple light scattering (Academic Press, New York, 1980).
[55] Derjaguin B.V., Muller V.M. and Toporov Y.P., Effect of contact deformations on the adhesion of particles, *J. Colloid Interface Sci.* **53** (1975) 314-326.
[56] Skalak R., Zarda P.R., Jan K.M. and Chien S., Mechanics of rouleau formation, *Biophys. J.* **35** (1981) 771-781.
[57] Lin M.Y., Klein R., Lindsay H.M., Weitz D.A., Ball R.C. and Meakin P.J., The structure of fractal colloidal aggregates of finite extent, *J. Colloid Interface Sci.* **137** (1990) 263-280.
[58] Clark M.M. and Flora J.V.R., Floc restructuring in varied turbulent mixing, *J. Colloid Interface Sci.* **147** (1991) 407-421.
[59] Allain C. and Jouhier B., Simulation cinétique du phénomène d'agrégation, *J. Phys. France* **44** (1983) L421-428.
[60] Von Smoluchowski M., Versuch einer matematischen theorie der koagulationskinetic kolloider losungen, *Z. Phys. Chem.* **92** (1916) 129-135.
[61] Snabre P. and Mills P., II. Rheology of weakly floculated suspensions of viscoelastic particles, *J. Phys. III France* **6** (1996) 1835-1855.